Journal of the European Ceramic Society 36 (2016) 631–644

Contents lists available at www.sciencedirect.com

Journal of the European Ceramic Society

journal homepage: www.elsevier.com/locate/jeurceramsoc

Glass ceramic sealants belonging to BAS ($BaO–Al_2O_3–SiO_2$) ternary system modified with B_2O_3 addition: A different approach to access the SOFC seal issue

Maviael J. Da Silva [a], José F. Bartolomé [b,*], Antonio H. De Aza [c], Sonia Mello-Castanho [a]

[a] Nuclear and Energy Research Institute, IPEN-CCTM, 2242 Lineu Prestes Av, Campus USP, 05508000 São Paulo, SP, Brazil
[b] Instituto de Ciencia de Materiales de Madrid (ICMM),Consejo Superior de Investigaciones Científicas (CSIC), Sor Juana Inés de la Cruz 3, 28049 Madrid, Spain
[c] Instituto de Cerámica y Vidrio (ICV), Consejo Superior de Investigaciones Científicas (CSIC), Kelsen 5, 28049 Madrid, Spain

ARTICLE INFO

Article history:
Received 7 July 2015
Received in revised form
30 September 2015
Accepted 4 October 2015
Available online 21 October 2015

Keywords:
Glass-ceramic
Sealants
Solid oxide fuel cell (SOFC)
Hot stage microscopy (HSM)
Phase equilibrium diagram

ABSTRACT

Four compositions in the $BaO–Al_2O_3–SiO_2$ system modified with B_2O_3 were investigated with regard to their use as glassy seals in anode supported SOFC or iT-SOFC. The glassy system studied contains varying percentages of SiO_2, Al_2O_3, B_2O_3, and high content of BaO as modifier (67–74%-wt). Their glass transition (Tg) and maximum densification point lies between 630 and 680 °C, and 734 °C to 828 °C, respectively. The viscosities of the four glasses are situated between 10^7 to $10^{9.5}$ Pa.s, in the sealing range (730–830 °C). Heat treatment at 850 °C, revealed crystalline phases identified as $BaAl_2Si_2O_8$ (hexacelsian) and $BaSiO_3$. The thermal expansion coefficient (TEC) of the obtained glasses (8.8–10.5 ppm/K) was comparable to zirconia (YSZ) electrolyte, and shows chemical compatibility and high characteristic bond strength (up to 33 ± 7 MPa). The compositions with higher BaO content in the system studied seem to be good candidates for iT-SOFC sealant application.

1. Introduction

Solid oxide fuel cell (SOFC) has emerged as one of the most challenging energy conversion technology because of its higher efficiency, and environment friendly nature [1–4]. Nevertheless, it is a common sense that the commercializing of the planar SOFC technology depends on the seals development [5–7].

Several glassy systems have been proposed each one showing different features, among these e.g. those based on alkaline earth metals such as barium. However because chemical interaction with metallic compounds as chromium, which typically comprises both metal interconnects (Crofer22APU mainly) and ceramics, degradation may occurs as a function of time allocated to highly volatile species consisting of chromium ($CrO_2(OH)_2$ and/or CrO_3), formed when the chromium oxide is in contact with gaseous oxidizing atmosphere react with barium oxide, producing barium chromate ($BaCrO_4$) having thermal expansion coefficient (TEC) around 22 ppm/K. As a consequence this thermal gradient would be disastrous for the integrity of the sealant.

Fortunately advances have been made in the last 10 years to reduce to acceptable levels the harmful effect of chromium volatilization [8–13]. The application of protective layers on the surface of the interconnectors has proven an effective method to inhibit the volatilization of Cr and its subsequent reactions with barium, as well as poisoning the cathode chambers at operational temperatures. The best results were obtained using $La_{0.9}Sr_{0.1}(CrO_3)$ layers at temperatures up to 900 °C. Around 850 °C, the kinetics of chromium vaporization is further reduced. Therefore the problem of Cr diffusion associated with ceramic systems containing barium has been successfully reduced [14–17].

From the above considerations the use of systems containing alkaline earth became widely feasible. The present work is an attempt to engineering, development, and selection of sealing glasses composition adequate for planar iT-SOFC sealing applications, based on the barium boron-aluminosilicate system ($BaO–B_2O_3–Al_2O_3–SiO_2$) chosen due its thermal–mechanical properties and desirable phase formation trend [18–20].

The ternary system $BaO–Al_2O_3–SiO_2$ is a relevant source for synthesis of new materials that presents valuable and at the same time, specific properties as corrosion resistance, mechanical strength, thermal stability, impermeability for gases and water, and even protection from ionizing radiation [21]. Compositions from this

* Corresponding author. Fax: +34 91 372 0623.
E-mail address: jbartolo@icmm.csic.es (J.F. Bartolomé).

http://dx.doi.org/10.1016/j.jeurceramsoc.2015.10.005
0955-2219/

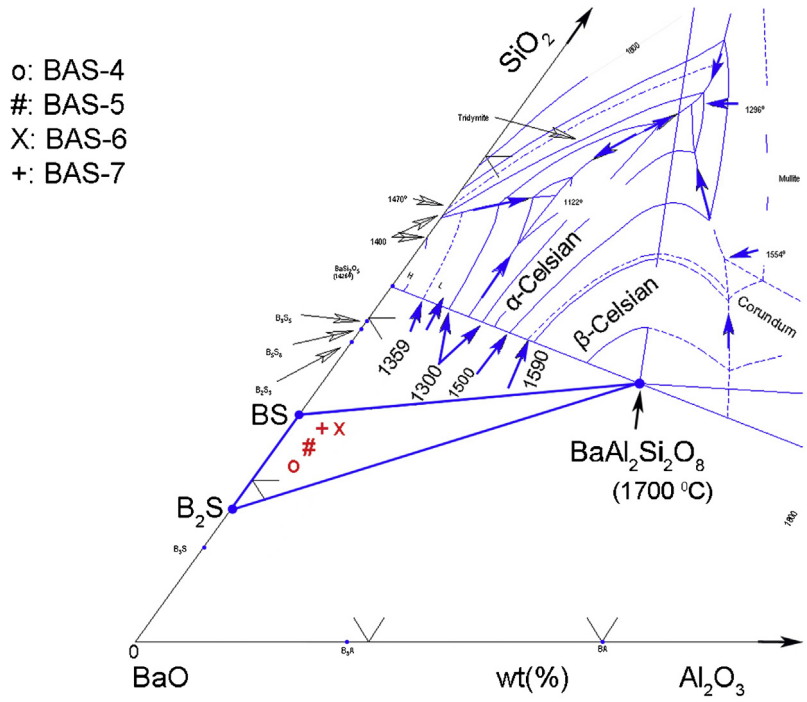

Fig. 1. Oxide modifier rich part of the BaO–SiO_2–Al_2O_3 equilibrium diagram with the batch compositions and the compatibility triangle (BS–B2S–BAS2); B = BaO, A = Al_2O_3, S = SiO_2. Adapted from [23,25].

system that presents considerable mechanical strength (up to 100 MPa) are found throughout the BaO–Al_2O_3–SiO_2 phase diagram. These specific advantages have leaded to a progressive use of glass-ceramics originated from this system, in a wide variety of applications like coatings, reinforced glasses, and sealings [21–23]. The *subsolidus* region of the BaO–Al_2O_3–SiO_2 system in a temperature interval of 1200–1400 °C, was choose due to the fact that the main desirable phase-formation processes occur within this temperature range [24–26].

On the other hand, the use of BaO–SiO_2–Al_2O_3 system or glass applications requires high melting temperatures [27]. Because of this, it is necessary the addition of a *flux* to reduce the processing temperature-within practical limits (≤1500 °C). Consequently, in order to reach adequate viscosity to cast the melt glass, part of the glass-forming SiO_2 was replaced by B_2O_3 [18].

2. Material and methods

2.1. Materials

For glass making SiO_2, and Al_2O_3 were used as oxides, H_3BO_3 was used as the source for B_2O_3 and Ba(OH)$_2$ for BaO. Powders of technical grade SiO2 (>99.5%) and of reagent grade of BaO (Merck) and H_3BO_3 (Merck) were used for preparation of the glasses.

2.2. Glass compositions criteria

Four glass compositions labeled BAS-4, BAS-5, BAS-6, and BAS-7, belonging to BaO–SiO_2–Al_2O_3 (BAS) system. The equilibrium diagram (Fig. 1) used as reference materials under equilibrium conditions falls within the compatibility triangle Δ(BS–B2S–BAS2) that have potential to crystallization of barium silicate phases such as $BaSiO_3$(BS), Ba_2SiO_4(B2S), with high thermal expansion coefficients (about 10–14 ppm/K) and $BaAl_2SiO_8$, hexa-celsian phase (up to 8 ppm/K) [22].

In these compositions, the amount of BaO (RO as modifier oxide) ranges around 70 wt% and Al_2O_3 (intermediate oxide) ranges between 3 and 6% wt. The addition of Al_2O_3 stabilizes the glass against most environments as well act as a glass former and contribute to the 3-dimensional connectivity in aluminosilicates glass compositions.

Table 1
Selected batch compositions (%-wt) of the glasses with their labeling: BAS-4, BAS-5, BAS-6, and BAS-7.

ID	BaO	B_2O_3	SiO_2	Al_2O_3
BAS-4	74	4	19	3
BAS-5	72	3	20.5	4.5
BAS-6	67	10	17	6
BAS-7	69	9	17.5	4.5

In order to reach adequate viscosity to cast the melt glass, part of the glass-forming SiO_2 was replaced by B_2O_3 as similar function oxide. These are combination of qualities that can favorably be applied for seals [5,28]. The same procedure is depicted in the Table 1.

The Fig. 2 shows the batch compositions studied located on the barium rich part of the BaO–SiO_2–B_2O_3 phase diagram where the glass–ceramic compositions are located close to the quasi-binary line $BaSiO_3$–BaB_2O_4 [18]. This system has two congruently melting end-members, the eutectic point of this binary system (point D Fig. 2) is located at 940° ± 4 °C and 56 wt% BaO SiO_2.

Although BAS system has already proposed for SOFCs, mere novelty is no proof of value, the farewell performance at hostile's environments and mainly the approach based on phase diagrams analyses are highlights. In the isoplethal studies described in the previous analyses, we anticipate the crystalline phases which occurred during the firing of the melt under equilibrium conditions. Thus we can use the data obtained from the phase diagram analyses as a function of temperature. On eye tracking in the present state of the art of SOFC seal research, the only general conclusion that one can reliably draw from the available literature is: there is no single material that can be consider as universal sealant material for SOFC application [28].

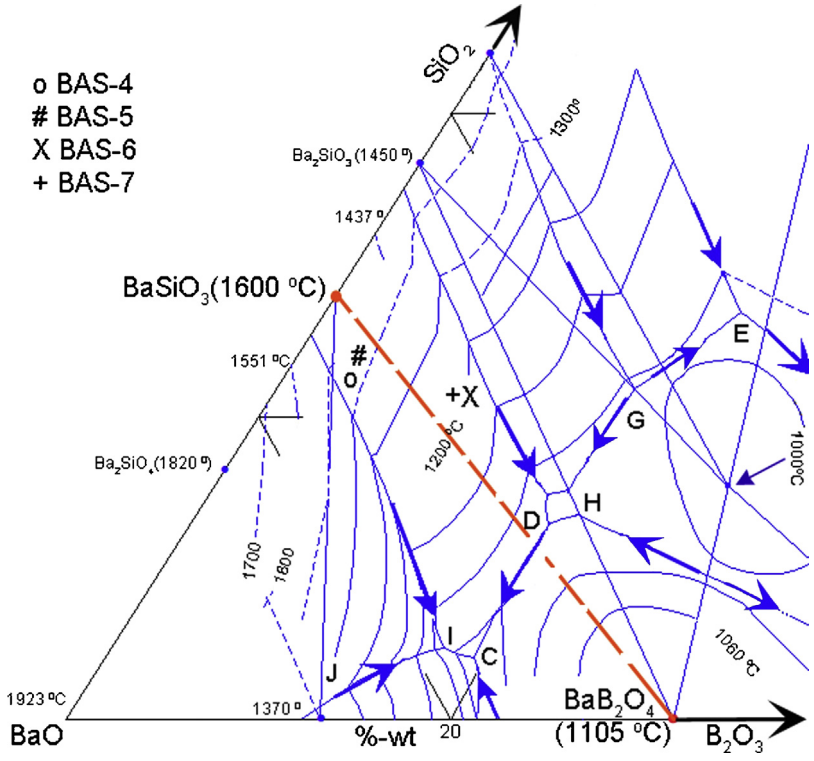

Fig. 2. Oxide modifier rich part of the $BaO–SiO_2–B_2O_3$ equilibrium diagram with the batch compositions, local eutetic (point H) at 940° ± 4 °C and 56% (wt%) de BaO SiO_2. Adapted from [28].

Finally without prejudice to the aforesaid, we argue that we have proposed a way forward to attack the seal problem. To summarize, the main criteria presently used for selection the glass composition include: (i) the presence of Barium silicate compounds due to its high TEC (10–12 ppm/K), mechanical strength (>100 MPa) and hexacelsian phase characterized by a considerable TEC (up to 8 ppm/K), (ii) the *liquidus* temperature effect promoted by B_2O_3 [29,30].

2.3. Experimental procedure

Batch formulations were calculated considering the weight losses for H_3BO_3 and $Ba(OH)_2$. Raw materials in adequate proportion for 40 g batch size were mixed, after mixing, the total mass was melted in an alumina crucible at 1500 °C for 2 h in a vertical furnace operated at a heating rate of 10 °C/min in air, and quenched in a preheated mould. Then the glasses were annealed at 50 °C below their glass transition temperature (T_g) to removal the thermal stresses. The bulk glasses were milled into powder in the range of 20–40 μm.

The Differential Thermal Analysis (DSC) of the glass powders were carried out in air (Setsys 16, SETARAM, France) at a heating rate of 10 °C min^{-1} to find out the characteristics temperatures. Glass powders were isostatically pressed (200 MPa) to cylindrical green samples of 1 cm in height and 0.6 cm in diameter. The thermal expansion coefficient (TEC) and sintering behaviour of the green and glass–ceramics samples after devitrification for 2 h at 850 °C were measured in air using a *DIL802 Bahr Germany* dilatometer with heating rate of 10 °C min^{-1}.

To verify the crystalline phases in the studied compositions after thermal treatment (850 °C for 2 h), samples were characterized by X-ray diffractometry (XRD) using a Bruker D8 model in the range of 10–70° (2θ) with step size of 0.02° s^{-1} with CuKα radiation as X-ray source.

A side view hot stage microscope (HSM) EM 201, with image analysis system and electrical furnace, 1750/15 Leica, was used. The measurements were conducted in air at heating rates of 10 °C/min on cylinder-shaped samples, 4 mm in height and 2 mm in diameter. The samples are placed on 10 × 15 × 1 mm alumina (>99.5%) supports. The sintering process of each glass was studied from the variation in area (A) of the samples as a function of temperature, as determined by the HSM software [31].

On the basis of the characteristic points obtained by hot stage microscopy (HSM) in the range $6 < \log(\eta) < 10$, (η in Pa.s), the experimental viscosity points were fitted to the Vogel–Fulcher–Tamman (VFT) Equation, the constants of the equation were calculated by linear regression. Then, fitting all the experimental figures with a function of the type $\eta(T) = A + B/(T–T_0)$, and changing the value of the constants A, B and T_0 until the highest level of the regression coefficient r^2 was obtained (≈99%) [32].

For studying the interface with zirconia (YSZ), glass cylindrical green body was joined with YSZ substrate at the temperature of 850 °C. Prior to the bonding, YSZ surfaces were polished down to 1 mm and ultrasonically cleaned with acetone and ethanol for 10 min. Microstructure near the interface (cross-section), was investigated on surfaces polished with silica carbide and colloidal silica suspension, by scanning electron microscopy SEM (Hitachi S-4300) coupled with energy dispersive spectroscopy (EDS).

The adherence behaviour of the glass–ceramic/zirconia interface was evaluated by the Shear bond strength (σ_s) using a mechanical testing machine (SHIMADZU AutoGraph AG-X, Japan) with a 5-kN load cell at a crosshead speed of 0.05 mm/min until failure. The load at fracture (F, in N) was recorded and the adhesion area (A, in mm^2) was measured. The σ_s results (in MPa) were calculated using $\sigma_s = F/A$. The shear bond strength results were averaged over 10 tests per composition.

After bond strength test, all fracture surfaces were analyzed using a stereomicroscope (Leica MZ6, Switzerland) for failure analysis. The mode of failure was classified as follows: cohesive failure (coating glass–ceramic remains on the substrate surface), and adhesive failure (delamination of the coating glass–ceramic from the zirconia substrate). Some specimens were further selected for

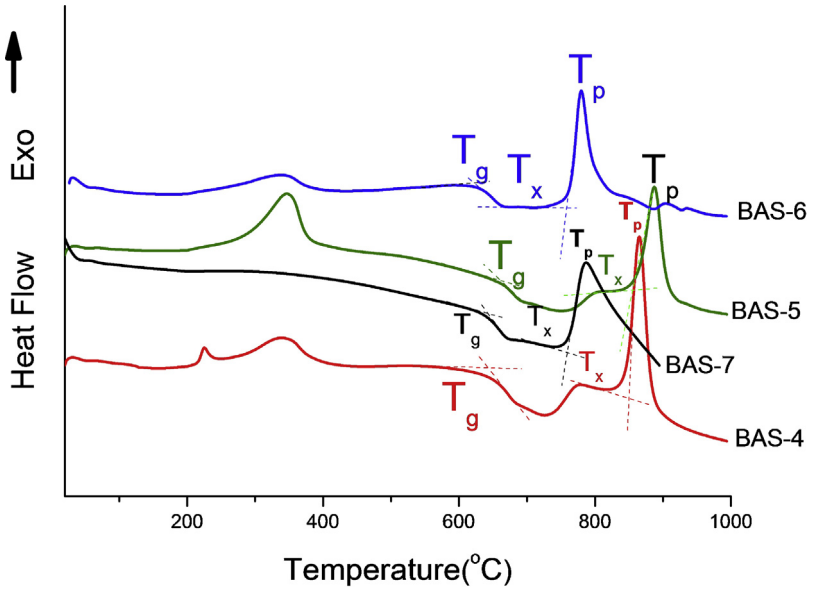

Fig. 3. DSC heating curves of BAS series glasses in air recorded at a heating rate of 10 °C min^{-1}. Where: T_g = glass transition temperature, T_x = onset of crystallization peak, T_p = maximum crystallization peak.

Table 2
Characteristics temperatures and TEC of the glass samples. Where: T_g = onset of glass transition temperature T_x = temperature of the onset of crystallization, T_p = temperature of the first crystallization exothermic peak, $\Delta T_x = T_x - T_g$ (Glass stability during heating), and $S_c = T_x - T_{MS}$(sinterability parameter).

Glass	T_g (°C)	T_x (°C)	T_p (°C)	ΔT_x (°C)	S_c (°C)	α_L TEC (RT to 700 °C (ppm/K))
BAS-4	643	850	865	207	80	9.7
BAS-5	678	857	886	179	76	10.5
BAS-6	670	756	782	86	24	8.8
BAS-7	680	758	788	78	−9	9.6

profilometer (Talysurf CLI 500, Taylor Hobson, Leicester, UK) that maps the surface by putting a stylus in mechanical contact with the sample. The arm has 90° conisphere diamond styli with 2 μm nominal radius tip. The data sampling interval in X and Y was 0.5 μm and 2.5 μm respectively. The resolution of Z-scale was 32 nm. Additionally, some fracture surfaces were selected for Scanning Electron Microscopy (SEM, Phenom G2, Netherlands) analyses.

3. Results and discussion

Fig. 3 depicted the DSC curves for all the glassy samples, and revealed that the glass transition occurs in range of the temperature from 640 to 680 °C. The exothermic reactions resulting from the release of energy during crystallization are represented by the exothermic peaks shown in Fig. 3: one crystallization temperature of great intensity (T_p) from 780 to 880 °C and the onset of crystallization (T_x) was also identified around 800 °C. This Figure also shows that the crystallization temperature increase with Al_2O_3 content (Table 1).

In this particular case, Al_2O_3 act as glass former producing an increase in T_g (onset of glass transition), and T_x (onset of crystallization peak) values [33,34]. The main results of this analysis are predicted in Table 2. The significant temperature difference $\Delta T_X = T_x - T_g = 179$ °C defined in terms of resistance to crystallization of a glass toward heating, shows by the sample labeled BAS-5, means a large ability of the glass to flow, accommodate mechanical stresses arising from possible TEC mismatch [34].

The X-ray diffraction patterns of the devitrified samples after 2 h at ~850 °C, temperature preliminarily defined from thermal analysis, are presented in Fig. 4. After devitrification, barium aluminosilicate (BAS2) was the predominant phase detected by XRD, along with $BaSiO_3$ (barium silicate(BS)). The patterns showed that Ba_2SiO_4 (barium orthosilicate(B2S)), also was formed.

The phase diagrams tell us that the compositions lies in the *subsolidus* region inside the compatibility triangle (BS–B2S–Celsian). This region of the diagram states that the equilibrium phases are BAS–B2S–Celsian [26]. A slight variation from phase diagram occurs and is related with shifting from equilibrium states due to kinetic effects. Particularly for this system, (BAS), where phase separation is facilitate by addition of boron [18].

The information supplied by means of $BaO–Al_2O_3–SiO_2$ ternary phase diagram (Fig. 1) support the analyses obtained by the XRD patterns (Fig. 4). For BAS-6 and BAS-7 samples, one of which with 10% and 9% (wt) of B_2O_3, respectively, one broad peak (2-theta ~ 14°) originated from BaB_2O_4 was observed, which is a typical feature of borate amorphous environment. The B_2O_3 compounds, in the glass compositions with small concentrations, below 9 wt%, were not detected by X-ray difractometer. The hump of the boron diffuse diffraction decreased until nearly vanished (BAS-4–BAS-5) due to crystallization of the glasses. The remaining diffraction lines pattern can be associated with a complex phase mixture consisting of barium silicates (pyro and ortho) and probably unreacted BaO.

Furthermore, the present data are consistent with those established for the $BaO–BaSi_2O_5–Al_2O_3$ subsystem, which verify the existence of celsian to hexacelsian inversion and Barium silicate–hexacelsian join. As a result, its appearance (hexacelsian) along with Barium silicates phases in the XRD spectra is fully justified [35].

The decrease in the area of the samples as a function of the temperature for all the glass samples studied by means of the Hot-Stage Microscopy (HSM) results is shown in Fig. 5. The shape of the normalized area versus temperature curves indicates that the BAS-4 and BAS-5 glasses soften over a considerable temperature range indicating glassy behavior [36]. There is a slight expansion behavior observed at the temperature range in which crystallization occurs (870–1050 °C). However, the samples BAS-6 and BAS-7 exhibit a constant trend until 1080 °C before wetting, which is a characteristic of materials exhibiting transformations towards heating, and

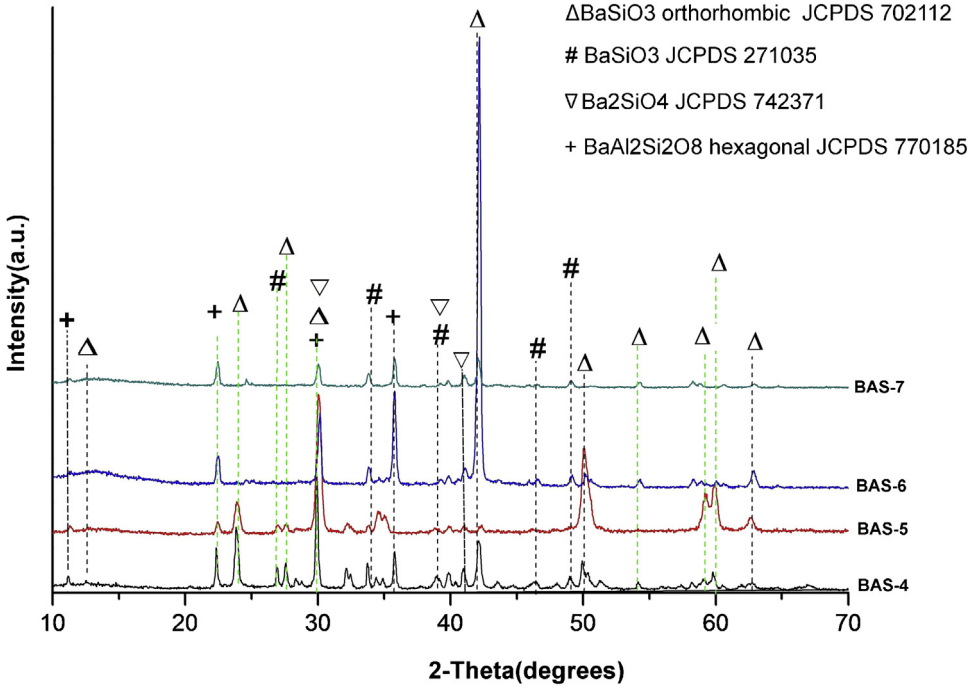

Fig. 4. XRD pattern of BAS series glassy samples heat treated at 850 °C for 2 h. The PDF files No 01-077-0185, 00-038-1450 and, 01-070-2112 which are corresponding to $BaAl_2Si_2O_8$ (hexacelsian), $BaAl_2Si_2O_8$(monoclinic), and $BaSiO_3$, respectively, are shown.

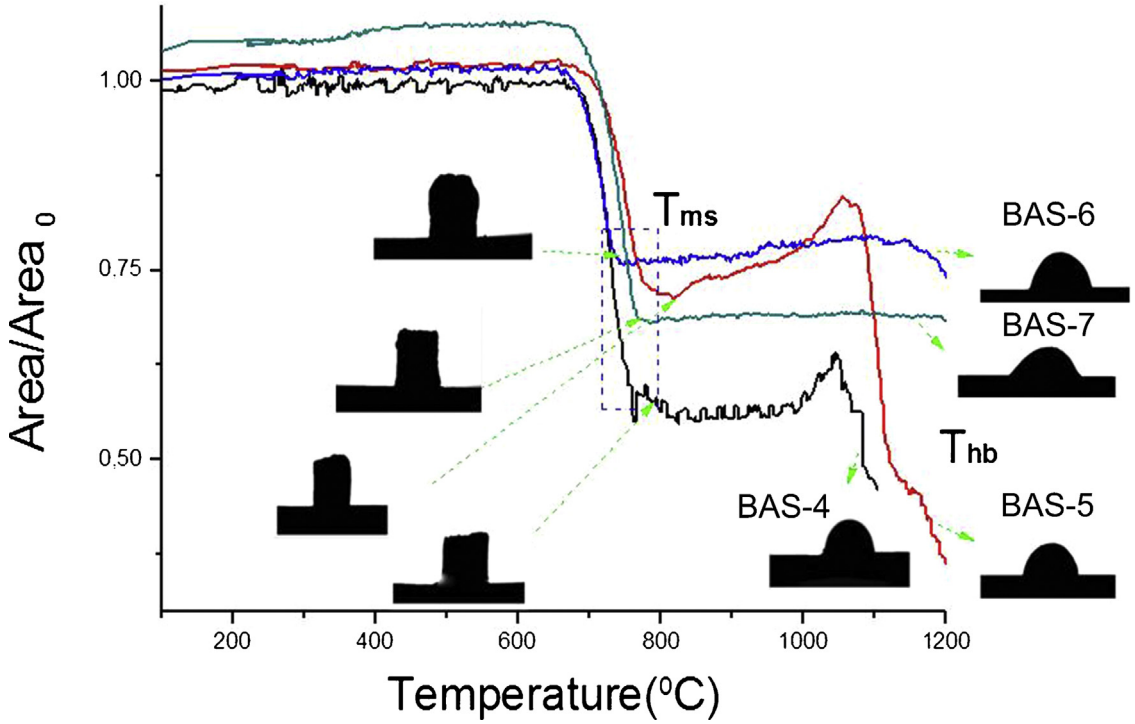

Fig. 5. Glasses compositions area variations (A/A_0) from HSM as function of temperature for the BAS series glasses. T_{MS} = temperature of maximum shrinkage and T_{HB} = half ball temperature.

also may indicate occurrence of significant crystallization for BAS-7 sample [37].

A comparison between DSC and HSM curves of all the investigated glasses obtained at a heating rate of 10 °C/min in the temperature range of 100–1000 °C (Fig. 6), reveals that sintering (temperature of first shrinkage = T_{FS} point), precedes the onset of crystallization (T_x) process in all studied glassy samples, except for the sample BAS-7 (Fig. 6d). The DSC/HSM combined curves shows that the onset of crystallization for BAS-7 glass (T_x = 759 °C) starts before the material has reached the maximum density (T_{MS} = temperature of maximum shrinkage = 765.12 °C), consequently inhibiting a complete sintering process. The considerably presence of crystals increases viscosity and consequently gives a partially incomplete densification of the glass-ceramic seal.

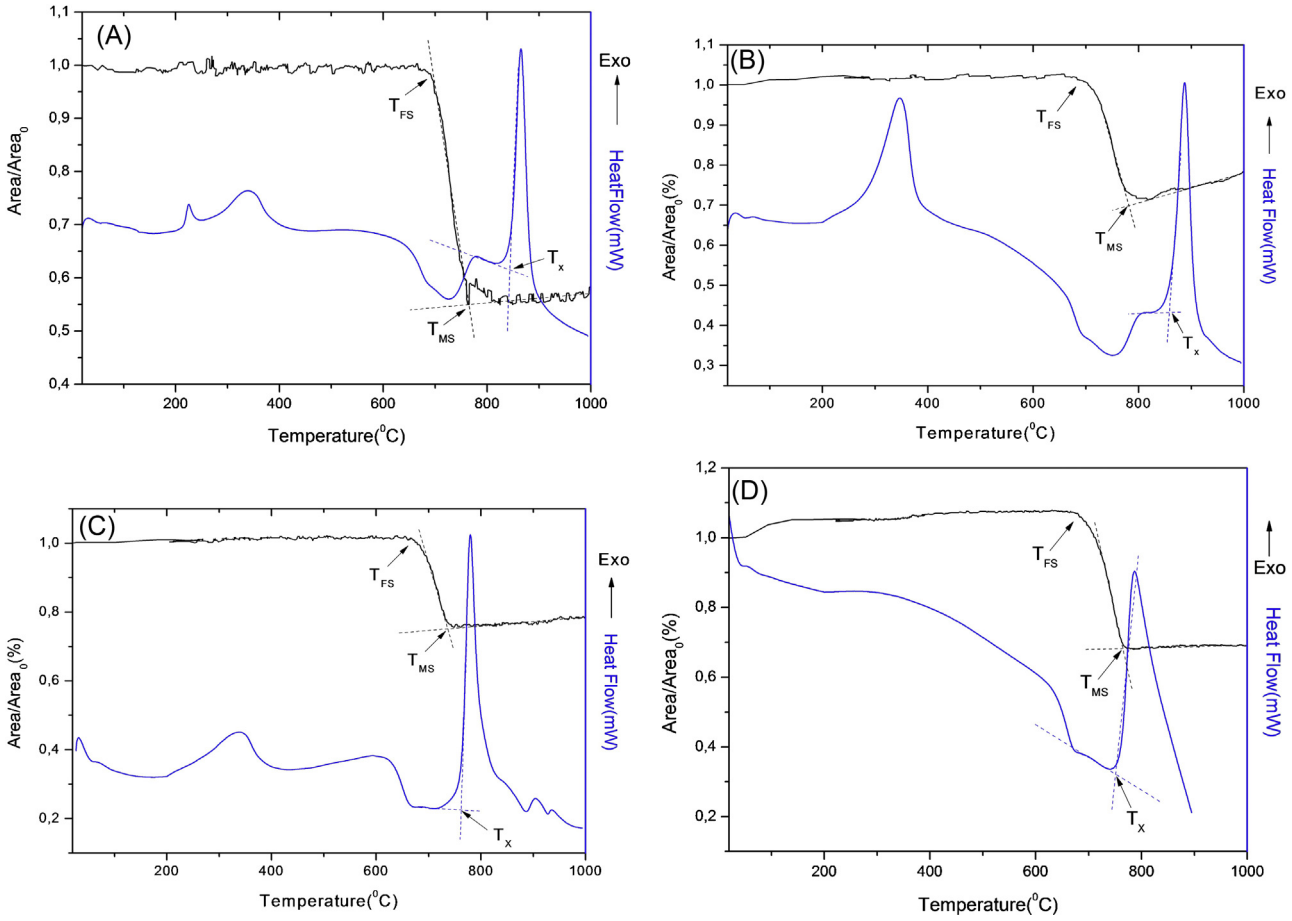

Fig. 6. Diferential Scanning Calorimetry (DSC) thermograms and glass compositions area variation (A/A_0) curve by means of Hot Stage Microscopy(HSM), obtained under same temperature scale and the same heating rate for samples: (a) BAS-4; (b) BAS-5; (c) BAS-6; and (d) BAS-7. T_{FS} = first shrinkage point, T_{MS} = temperature of maximum shrinkage and T_x = onset of crystallization peak.

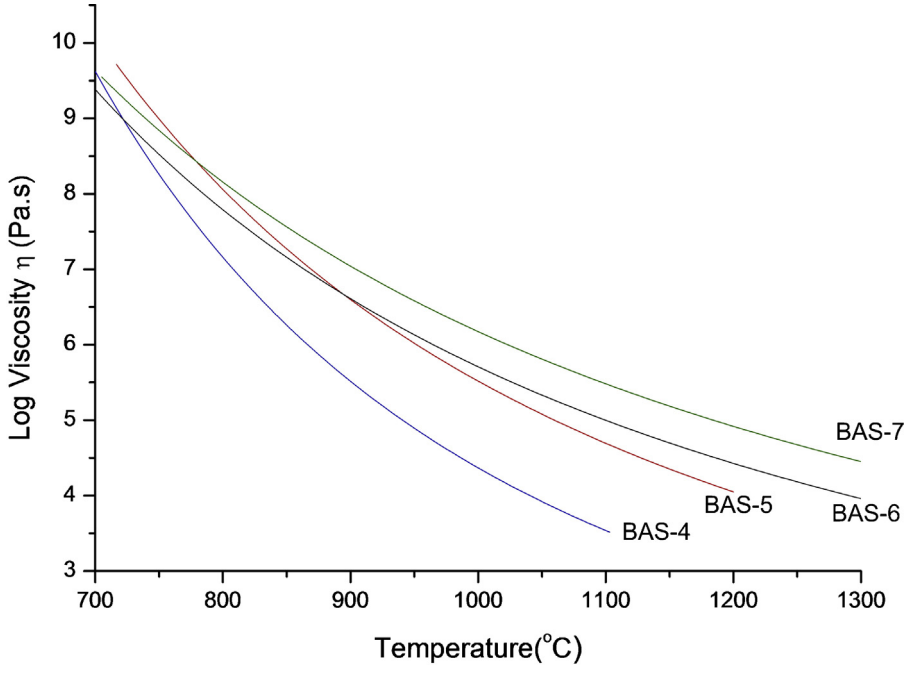

Fig. 7. Viscosity-temperature curve for all glasses obtained from Hot Stage Microscopy (HSM).

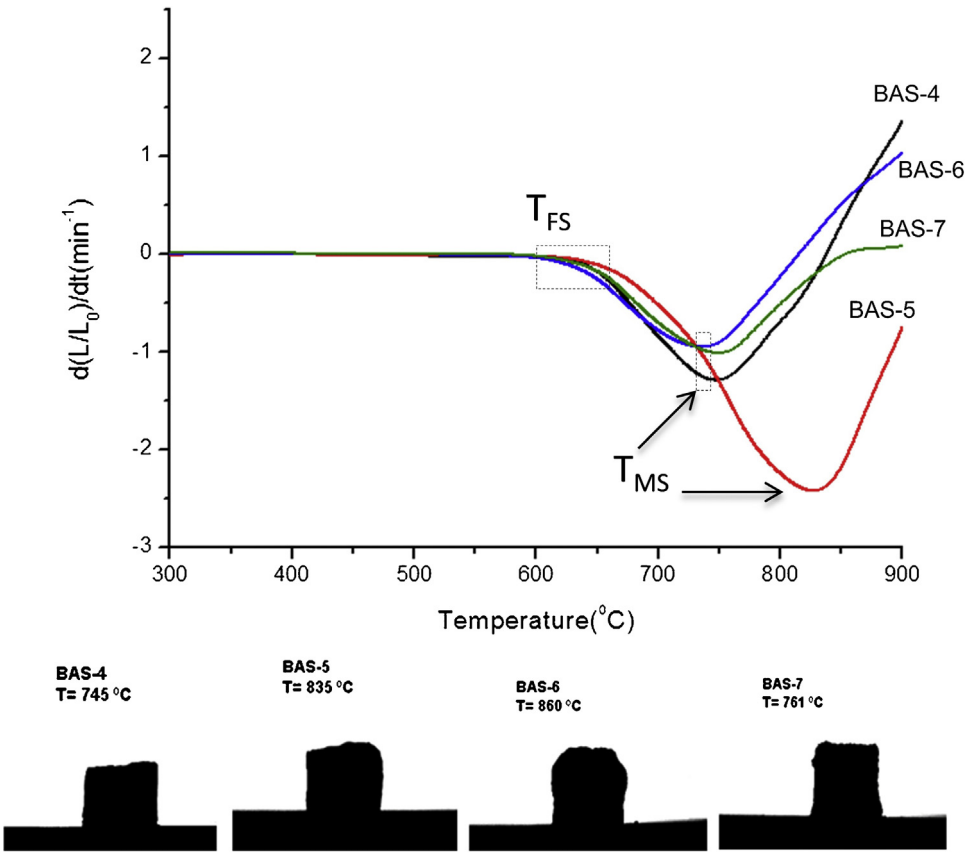

Fig. 8. Linear shrinkage rate *vs* temperature diagram for BAS parent compositions. T_{FS} and T_{MS} are the first and the maximum shrinkage points, respectively.

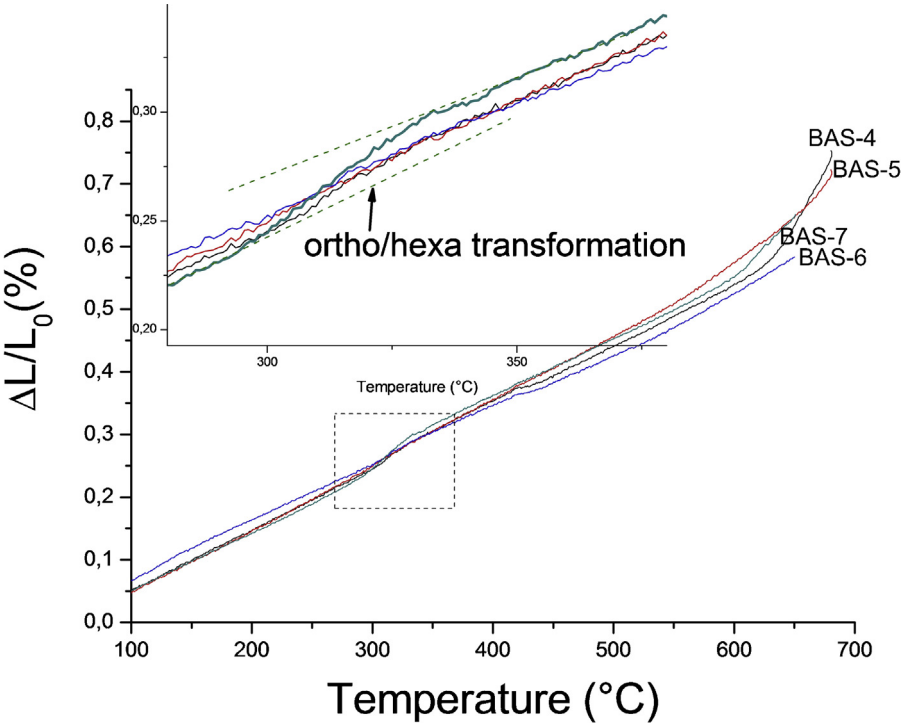

Fig. 9. Thermal expansion (TEC) curves of glasses measured between RT and 700 °C (RT to 700 °C (ppm/K)). Expanded area, temperature range: 250–400 °C, showing ortho-hexa transformation. Heating rate of 10 °C/min, in air.

Table 3
Results obtained for linear shrinkage as function of temperature at 1000 °C of the glassy systems BAS-4 BAS-5 BAS-6 and BAS-7 with constant heating rate of 10.0 °C/min

Glass	T_{FS} (°C)	T_{MS} (°C) $\frac{d}{dT}\left[\left(\frac{(L/L_0)}{dt}\right)\right] = 0$	Linear shrinkage rate $d\left[\frac{L}{L_0}/dt\right] \times 10^{-1}(min^{-1})$
BAS-4	645	745	12.9
BAS-5	653	828	24.2
BAS-6	634	734	9.5
BAS-7	654	753	10

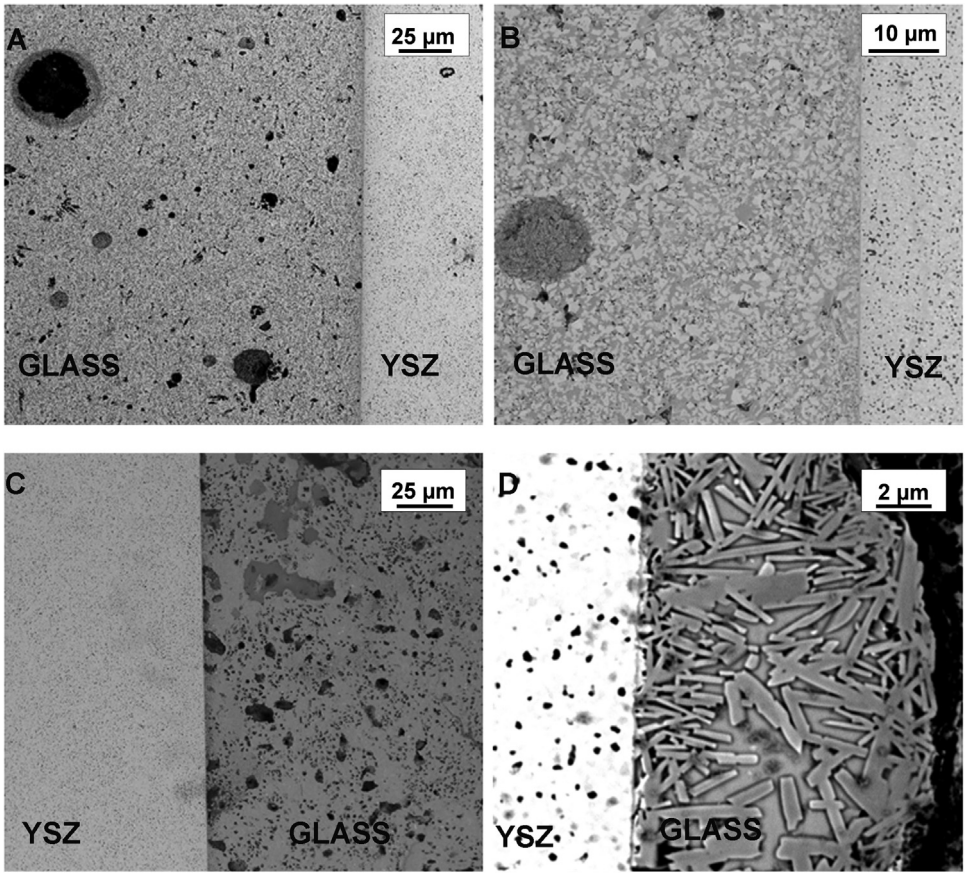

Fig. 10. SEM images of the polished glass–ceramic/zirconia interface cross-section of glass BAS-4 (a), BAS-5 (b), BAS-6 (c), and BAS-7 (d), after thermal treatment at 850 °C for 2 h.

Table 2 lists the characteristic temperatures for glasses as obtained by HSM (T_{FS} and T_{MS}) and DSC (T_g, T_x and T_p) accompanied with the values of sinterability parameter (S_c), where $S_c = T_x$ (onset of crystallization temperature)—T_{MS}. At this point is convenient to define this parameter by wish is possible to measure the ability of sintering in contrast to crystallization, the greater S_c more independent the kinetics of these processes are [32,37,38]. For BAS-7 sample (Fig. 6b) the onset of crystallization was located within the range of sintering temperature, thus S_c is negative. A negative S_c means that crystallization may hinderthe completion of sintering by increasing the viscosity of the material, glass sintering precedes crystallization in the remaining (BAS-4, BAS-5, and BAS-6) compositions, and consequently S_c is positive. Thus, it seems that well-sintered and at the same time partially crystallized glasses can be obtained. The Fig. 7 exhibits the viscosity of the four glasses as a function of temperature. The experimental points, derived from HSM images are situated between 10^7 e $10^{9,5}$ Pa.s, in the sealing range (730–830 °C) [31,32]. Although the rheological behaviour of the samples BAS-5 and BAS-7, are quite similar, can be verified in viscosity *vs*. temperature curves that the viscosity increases with Ba^{2+} content. For the BAS-6 sample, the content of B_2O_3 (10% wt) contributes to lower the viscosity, since the glassy oxide network of boron consists of two dimensional triangles, with no considerable linking in three dimensions which results in a fragile network connectivity. Spectra (MAS–NMR) obtained from BAS glasses series for additional applications (optical) performed with 29Si and 11B nucleus revealed that silicon, and boron atoms have mainly four-fold coordination [39]. These considerations help us to explain why the BAS-6 has the lowest viscosity values among the BAS parent glasses [40].

The viscosity of parent glasses BAS-4, BAS-5, BAS-6 and BAS-7, lies in the range of $\approx 10^7$–$10^{9.5}$ Pa.s at joining temperature (730–830 °C), and 10^6–$10^{7.5}$ at working temperature (900 °C) [41].

Since the Ba^{2+} field strength force(0.25 v.u.–valence units), is the lowest among alkaline-earth cations, and assuming that Ba^{2+} act as modifier in the glass network, high concentrations of divalent ions like Ba^{2+} weaker bonding at lower field strength [42]. Thereby resulting in decreased viscosity with Ba^{2+} content caused by gradients in field strength comes from this modifier ion (Fig. 7).

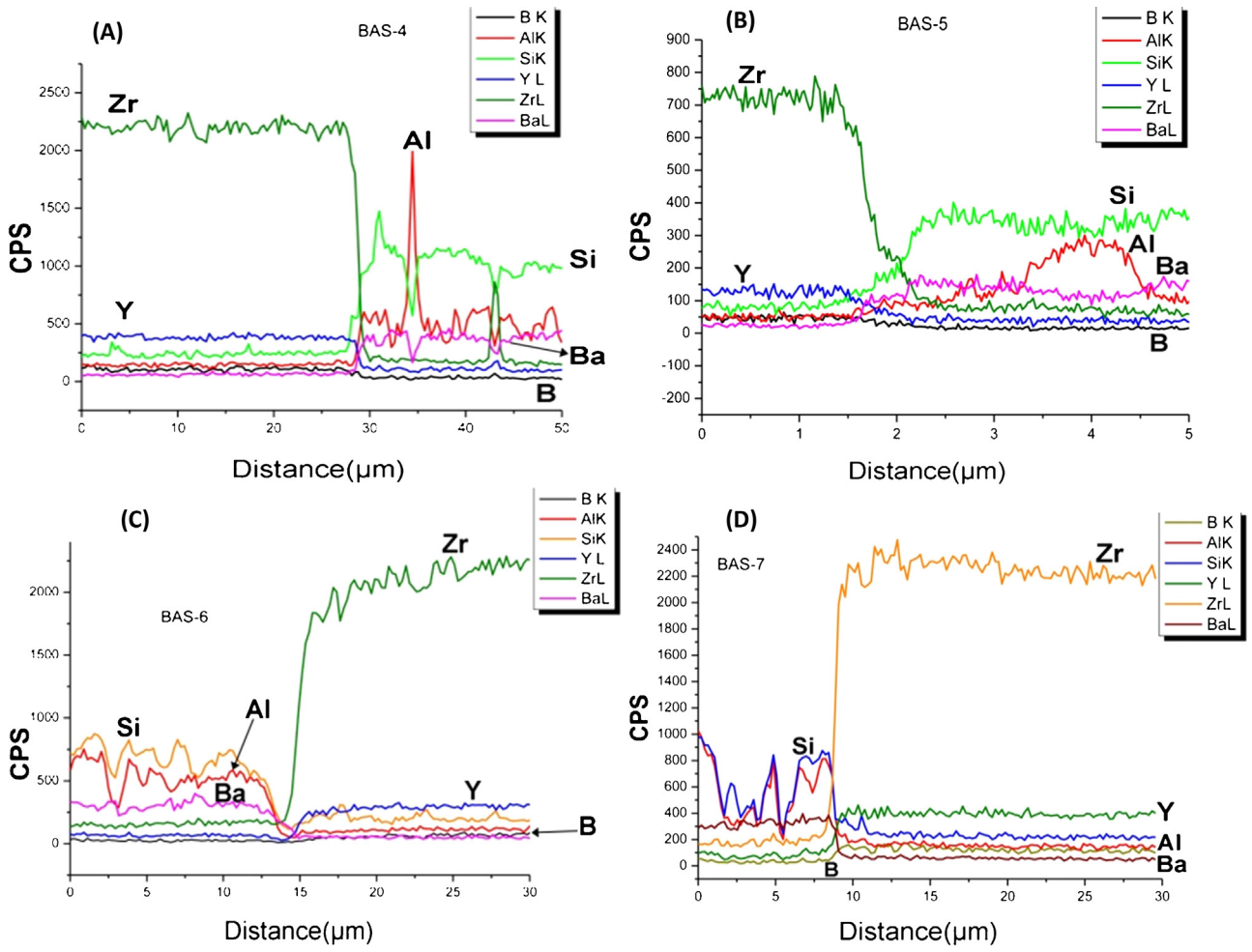

Fig. 11. X-ray line scanning of B, Al, Si, Y, Zr, Ba respectively, of the polished glass–ceramic/zirconia interface cross-section of glass BAS-4 (a), BAS-5 (b), BAS-6 (c), and BAS-7 (d).

Due to its low mobility a slower ion Ba^{2+} that finds itself in the region of lower field strength is slowed down to high field strength and then get back to the boundary, this is the so called "self-regulating effect" [43]. The lower the strength of the Oxygen-modifier bond, lower is the tendency to separate into two liquids. Thus viscosity measurements shall reflect the compositions of the liquid phase present and the effectiveness of the gradient in ionic field strengths (ΔIFS) between the glass former and oxygen and the modifier cation and oxygen [44].

In order to investigate the shrinkage behavior of the glass-samples in detail, and consequently determine T_{seal}, the sintering shrinkage rate curve for the BAS glass ceramics series was plotted (Fig. 8). The sealing temperature (T_{seal}) defined as the temperature at which the densification and sintering reach the maximum for a given material is an important parameter in the design of sealants, since these materials should be tight at working temperature of the cell. This temperature is dependent of the melt compositions.

The choice of particle size can affect the sinterization by transport mechanisms involved in compounds formation or by distribution of the particles throughout the melt. In one hand small particle sizes (<20 μm) of glass powder accelerate melting, homogenization and densification. But in the other hand, the use of very fine particles has associated problems too: lower resistance to crystallization indicating more difficult to control crystallization and tendency of glasses to collapse before adhering to the substrate [34,45].

The heating heat for the experiments in the present study were performed at 10 °C/min where its contraction was initially rapid and then more slow as it approached near full density [46]. We do not advocate faster or slower heating heats for essay involving glass samples. Rather, we advocate a moderate rate allowing it sufficient time to accommodate naturally to the next temperature.

According to sintering shrinkage rate plots (Fig. 8), glasses BAS-4, BAS-6, and BAS-7 have shrunk to almost the same rate (around 10×10^{-1} min^{-1}). There are slight changes in shape of the samples evident from the inset photographs of Fig. 8 and there is a shift in the temperature of first shrinkage (T_{FS}) for BAS-4, BAS-5, and BAS-7 (around 650 °C) in relation to BAS-6 (634 °C).

In addition, we can observe from Fig. 8 that maximum shrinkage (T_{MS}) of glass BAS-5 has occurred at 828 °C whereas for the remaining samples the same point of shrinkage has occurred at 734 °C (BAS-6) and around 750 °C (BAS-4–BAS-7). This peak in shrinkage rate curve corresponds to the increased densification due to liquid-phase sintering, which is characterized by the rearrangement of the particles and the viscous flow of the melted glassy phase. Therefore it is clear that the addition of boron oxide has reduced the softening point of these glasses. The presence of a liquid phase capable of dissolving some of the solid particles produces a mass transport path that is geometrically the same that grain boundary produce in the sintering process involving only the solid phase. This is the case for the samples BAS-6 and BAS-7 that contains a considerable amount of B_2O_3 (10% and 9% wt, respectively), the presence

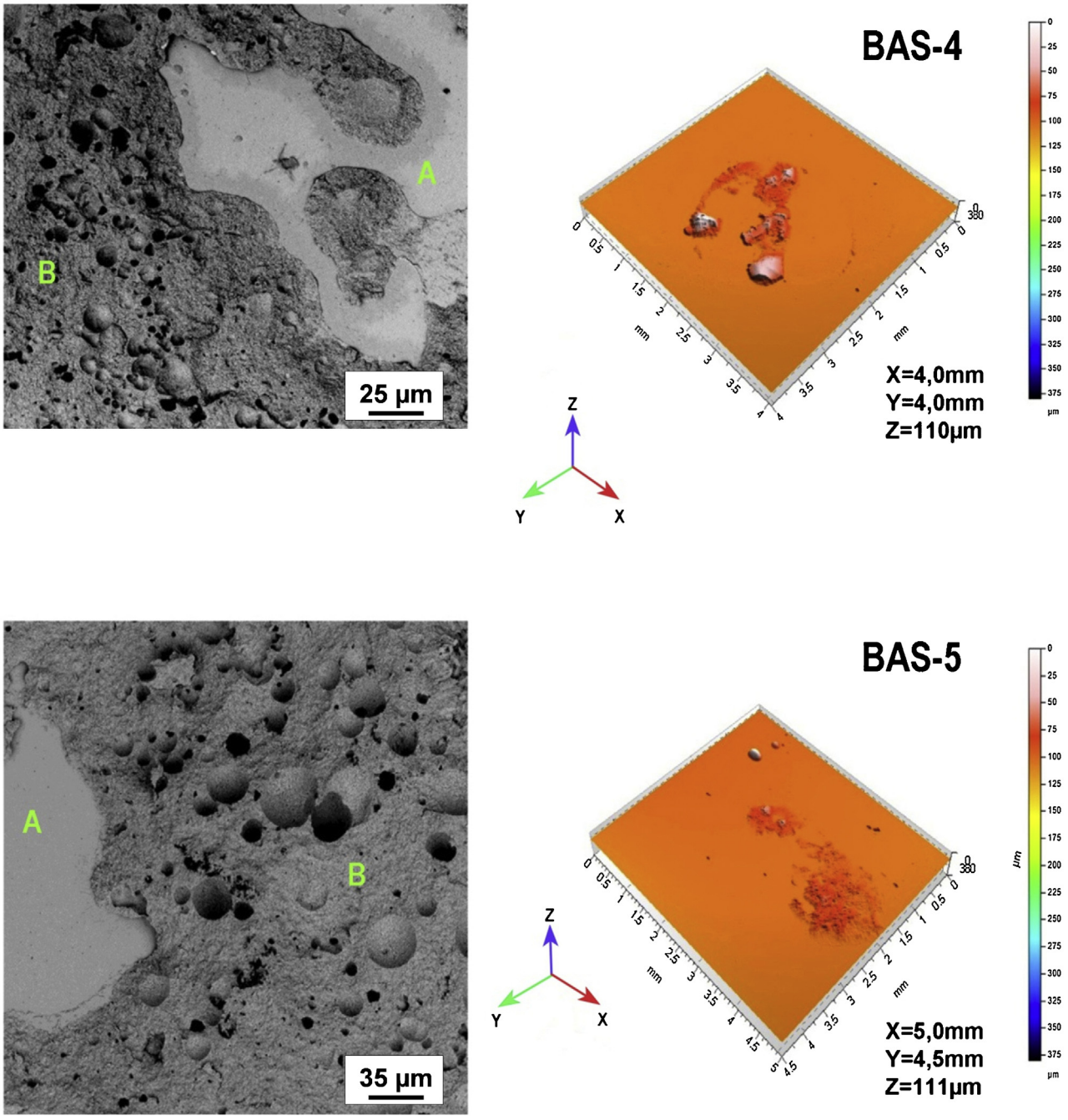

Fig. 12. Failure patterns, SEM micrograph (left side) and 3D profilometer image (right side), for BAS-4 and BAS-5 coating glass-ceramic (Region B) on YSZ substrate (Region A).

of this compound can accelerate an alternative mechanism of mass transport.

During sintering, shrinkage started at 653 °C (BAS-5 glass sample) and had a single maximum around 830 °C. For the glasses BAS-4, BAS-6 and BAS-7 the sinter process started approximately at the same temperature, but the sintering rate was lower and reaches a maximum at lower temperatures: 745 °C, 734 °C, and 753 °C, respectively. In other words, in the process of linear shrinkage during liquid phase sintering, the first and faster shrinkage step occurs when the liquid component is melted (B_2O_3), and the amount of shrinkage depends on the volume of liquid that is formed [38].

As a result, slower shrinkage rates (BAS-4, BAS-6, and BAS-7), occur probably because numerous points of contact of a particle with the adjacent begin to compete with each other for diffusing through the melted glassy matrix. White elongate crystals morphology growing in the amorphous material, e.g.: BAS-7 sample (vide Fig. 10d), attributed to barium silicate phase, competed with each other during growth by means of interactions between neighboring needles-shaped crystals, and darker needle shaped crystals in the amorphous matrix attributed to hexacelsian [47]. The gray areas possibly are the residual amorphous glass phase consisting of barium-boron-silicate. Surface diffusion competes with densification mechanism and lead to coarsening (grain growth) of the microstructure. In other words, the sintering mechanism involves interplay between densification and coarsening and increases the average pore size, consequently reduces the rate of shrinkage. The

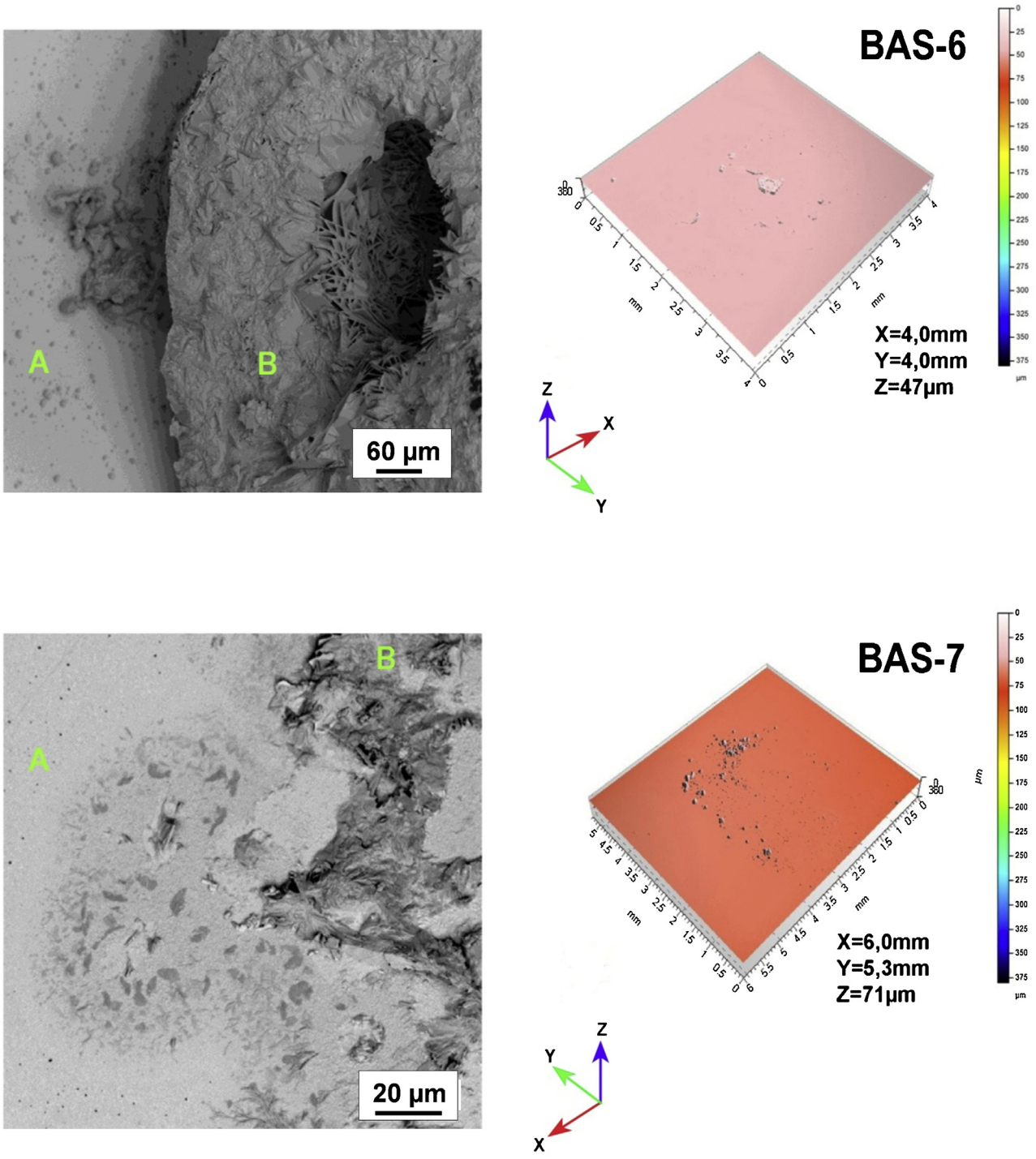

Fig. 13. Failure patterns, SEM micrograph (left side) and 3D profilometer image (right side), for BAS-6 and BAS-7 coating glass-ceramic (Region B) on YSZ substrate (Region A).

linear shrinkage point of maximum is the point where grain growth (coarsening) starts to become significant.

As is listed (Table 3) the sintering rate of the specimens BAS-6, and BAS-7, which includes the highest B_2O_3 content in all samples, is lower than the other two remaining samples (BAS-4 and BAS-5). This clearly indicates that B_2O_3 composition plays an important role in the decrease of the sintering rate. As a result the densification, at lower temperatures, was enhanced by the liquid phase. Whereas, the remaining group with lower B_2O_3 (4% wt and 3% wt, BAS-4 and BAS-5, respectively) achieved more rapid densification. For glassy systems which grain boundaries cannot exist, the densification occurs by viscous flow, and if crystallization occurs during sintering (Fig. 8) the viscous flow is impeded. The interaction between kinetic of crystallization and densification can result in microstructures with accentuated level of porosity (e.g., BAS-7). This competition between the contacts of the particle causes a decrease in the linear shrinkage rate of both, the solid and the liquid phase sintering [48].

For sintering behavior too high Ba^{2+} content (BAS-4) is detrimental, probably due to saturation. Table 3 summarizes the results

obtained for linear shrinkage as function of temperature for all vitreous samples. It is important to notice that according to these results, the optimum sintering temperature or the maximum densification is an indication of the suitable joining temperature to a specific composition.

It is well know that barium borate can be normally used to decrease the sintering temperature of glass-ceramic as a flux agent because of its low-melting properties [46]. Although, only the presence of $BaO–B_2O_3$ compounds cannot interfere totally on the physical properties of the melts, opposite effects on the sintering kinetics may occur such as decelerating the sintering kinetics by crystallization. The presence of high BaO compositions (>70% wt, BAS-4) results in formation and subsequent growth of barium silicate crystals and residual Ba^{2+} not reacted.

The dilatometric curves of the barium boron aluminosilicates glass system devitrified after 2 h at 850 °C are shown in Fig. 9. Thermal Expansion Coefficient (TEC) values are summarize in Table 2. As is well know, the presence of β-cristobalite phase in the $BaO–Al_2O_3–SiO_2$ system, results in a inflexion in the Thermal Expansion Curves from β to α structure type at about 200 °C. There is no such inflexion at 200 °C, and in fact, the formation of Cristobalite must be avoid because cause cracking at conditions of high temperatures. It also found that the hexacelsian phase (inflexion around 300 °C) can be a trigger to a reversible structural transformation into orthorhombic form followed by a volume change around 3% [49].

The formation of undesirable celsian phase was retarded probably due to the high kinetic barrier associated with the transformation from hexacelsian to celsian [50], as a result the curves are smooth and do not show considerable signs of transformation, except the sample BAS-7 that exhibits discontinuity around 300 °C, due to the ortho ↔ hexa transformation [51].

In a first approximation, the dilatometric curves were linear in a wide temperature range, in other words the TECs did not depend much on temperature. The values of the respective TEC in the temperature range from RT to 700 °C (iT-SOFC-working temperature) vary from 8.8 to 10.5 ppm/K in a range acceptable for components of sealing materials in intermediate temperature fuel cells: YSZ electrolyte and Ni-YSZ anode (10.5 ppm/K), LSM (La–Sr–Mn) Cathode (12.2 ppm/K) [28]. This means that if the respective crystalline phases are combined with other crystalline or residual amorphous phases, an appropriate TEC can be adjusted, mainly for BAS-5 and BAS-4 glasses. The expansions measured by dilatometric essays are strongly affected by the structural environment of the samples [52].

Earlier results obtained by FT-IR and MAS–NMR spectra [39] showed that the BAS glasses series main network were constitutes of Q2 units, and B_2O_3 formed the triangular BO_3. Addition of BaO up to 70% (wt) produced relevant modifications in the distribution of Q units. The increase of the Q1 and Q3 species at detrimental of Q2 units parts, is one of those modifications [53–56].

The higher Al_2O_3/B_2O_3 ratio (1.5), presents by BAS-5, authorize that B^{3+} ions go to react with Al_2O_3 by forming the tetrahedrons AlO_4 and the remainder will react with B_2O_3 producing non-bridging oxygen (NBO), consequently has to weaken the vitreous network and expansion has to increase.

Since the BAS-5 glass gets better TEC for ratios $[Al_2O_3]/[B_2O_3] = 1.5$, BaO concentration should not be chosen larger than 72% wt in order to avoid that BO_3 units re-converted into BO_4, strengthening the network and as result thermal expansion decreases with modifier. Reversal trend is observed for BAS-6 and BAS-7 samples (<70% wt BaO). This effect is called “boron anomaly”, depending on the glass composition, boron assume three or fourfold coordination [45–46].

The TEC obtained (8.8 to 10.5 ppm/K) are very near to YSZ electrolyte. Hence, from the expansion mismatch point of view, the compositions are suitable as sealants for SOFC applications [11,57–59]. Therefore, the compositions confirm the behavior as predict by the phase diagram as well as designed.

The SEM micrographs of the polished cross-section of the glass–ceramic/zirconia interface, after thermal treatment at 850 °C for 2 h are shown in Fig. 10. The glasses show chemical compatibility with zirconia, where no interfacial reaction was detected. A tendency toward immiscibility and the presence of droplets shaped immiscibility regions of small dimensions, which are either solid or hollow, can be observed in the BAS-4 (Fig. 10a) and BAS-5 (Fig. 10b) samples microstructures. It can be seen that the nucleation and growth of crystalline phase has taken place in the glass matrix [60]. These types of phases are developed during controlled crystallization by providing heat treatment between glass transition (T_g) and melting temperature (T_m).

In the case of the polished cross-section of the BAS-6 (Fig. 10c) and BAS-7 (Fig. 10d) samples, the dark zones probably have glassy boundary to the formed crystals. Some flake-like particles can also be observed. The de-vitrified glasses are composed of the main phases: $BaSiO_3$ bright elongated crystals growing within the glass matrix, and $BaAl_2SiO_8$ needle-shaped dark grey crystals [47,61]. In sample BAS-7crystallization process starts uniformly and crystalline growth is taking place in different bands apparently segregate to the surface (Fig. 10d).

The extent of diffusion of constituent elements from the YSZ into the glass and vice-versa has been observed through EDS line scanning (Fig. 11). All the Glass seals bonded well to the YSZ substrate and no gaps or microcraks were observed even at the edges of the joints. The relative concentration profile of Ba is approximately constant across the interface suggesting the absence of diffusion barriers for this element. A good wetting regime and continuous interfaces with minimal reaction zones, no cracks or gaps, were revealed after cross-section and polishing. No significant diffusion of Ba into the YSZ or formation of B-rich reaction product was observed [62,63].

Typical failure patterns in the shear strength test for the specimens are shown in Figs. 12 and 13. BAS4 and BAS5 samples (Fig. 12) show mainly cohesive failure i.e., coating glass-ceramic (region B) remains on the substrate surface (region A). A close look at the failure mode showed that this was not straightforward. On the other hand, BAS-6 and BAS-7 (Fig. 13) show adhesive failure (delamination of the coating glass–ceramic from the substrate ceramic) [64,65]. The crack can propagate though the weakest layer that in this particular case is the interface. The BAS 5 specimens exhibited the highest characteristic bond strength (33 ± 7 MPa), followed by the BAS 4 (19 ± 4 MPa) and the BAS 6 and BAS 7 samples (9 ± 2 and 4 ± 1 MPa respectively).

The bonding properties between the substrate and the sealant may be related with the BaO content. It was expected that the zirconia substrate and the sealant should have similar TECs to produce a stable bond. Therefore the joining temperature and the thermal stress induced by it are critical parameters to select a seal [7]. For all the samples, the thermal stresses induced are very similar. So the difference between the values of bonding strength must be related with higher crystallization process of the BAS 6 and BAS-7 samples ($BaSiO_3$ elongated crystals and $BaAl_2SiO_8$ needle-shaped crystals), that reduce strains [64].

4. Conclusions

New glass ceramics in the $BaO–Al_2O_3–SiO_2$ system modified with B_2O_3 were investigated for sealing iT-SOFCs at temperature range of 700–850 °C.

The sealing temperature (T_{seal}) for all the compositions has occurred in the range of 730–830 °C, This temperature is dependent of the melt compositions.

Devitrification heat treatment at 850 °C, which is in the intermediate operation temperature range of SOFCs revealed crystallization, and phases were identified by XRD as $BaAl_2Si_2O_8$ (hexacelsian), and pyro–ortho barium silicates.

Crystallization process that take place in the glass–ceramic compositions with BaO content (69% wt) studied in this work, inhibits the complete sintering process of the sample. Therefore, the considerably presence of crystals in these compositions increases viscosity and consequently gives a partially incomplete densification of the glass-ceramic seal ($S_c = -9$).

The thermal expansion coefficient (TEC) of the obtained glass-ceramic after devitrification heat treatment was comparable to zirconia (YSZ) electrolyte (8.8–10.5 ppm/K), and shows chemical compatibility (no interfacial reaction was detected by SEM–EDS). Adhesion test revealed homogeneous interface between the glass–ceramic and the YSZ electrolyte. The fracture pattern of the glass ceramic specimens with higher BaO content was mainly cohesive and with higher values of shear strength (19 ± 4 and 33 ± 7 MPa respectively), while glass-ceramics with lower BaO content and therefore higher crystallization process, demonstrated higher percentage of interfacial failure and lower values of shear strength (9 ± 2 and 4 ± 1 MPa respectively).

In conclusion, the compositions with higher BaO content, in the system studied in this paper are found to be promising candidates for sealing at moderate temperature (700–850 °C) in planar SOFC application. For the particular case of BAS-5, shown compatible CTE with YSZ, such combination of pyro and ortho-barium silicate phases along with a minor concentration of hexagonal celsian phase crystallizes and favors TEC matching, micro-structural stability, and desirable mechanical properties. Because of this BAS-5 glass is the most promising sample for SOFC sealing application.

Acknowledgments

This research was performed with support from the Brazilian government through their respective funding agencies CAPES and CNPq (Conselho Nacional de Desenvolvimento Científico e Tecnológico), as part of the Science without Borders(CsF-SWE) scholarship program (Project No.237958/2012-0), FAPESP, and the Spanish government under Project No MAT2013-48426-C2-1-R. We would like to acknowledge the help of Mr. Luis Contreras in the course of the Hot Stage Microscopy(HSM) analyses.

References

[1] A.J. Appleby, Fuel cell technology: status and future prospects, Energy 21 (1996) 521–653, http://dx.doi.org/10.1016/0360-5442(96)00030-8.
[2] N. Minh, Solid oxide fuel cell technology-features and applications, Solid State Ionics 174 (2004) 271–277, http://dx.doi.org/10.1016/j.ssi.2004.07.042.
[3] Wincewicz K.C., Cooper J.S., Taxonomies of SOFC material and manufacturing alternatives, 140, (2005), 280-296, 10.1016/j.jpowsour.2004.08.032.
[4] E.I. Wright, S. Rahimifard, A.J. Clegg, Impacts of environmental product legislation on solid oxide fuel cells, J. Power Sources 190 (2009) 362–371, http://dx.doi.org/10.1016/j.jpowsour.2009.01.069.
[5] J.W. Fergus, Sealants for solid oxide fuel cells, J. Power Sources 147 (2005) 46–57, http://dx.doi.org/10.1016/j.jpowsour.2005.05.002.
[6] M.K. Mahapatra, K. Lu, Seal glass for solid oxide fuel cells, J. Power Sources 195 (2010) 7129–7139, http://dx.doi.org/10.1016/j.jpowsour.2010.06.003.
[7] D.U. Tulyaganov, A.A. Reddy, V.V. Kharton, J.M.F. Ferreira, Aluminosilicate-based sealants for SOFCs and other electrochemical applications—a brief review, J. Power Sources 242 (2013) 486–502, http://dx.doi.org/10.1016/j.jpowsour.2013.05.099.
[8] Y. Liu, D.Y. Chen, Protective coatings for Cr_2O_3-forming interconnects of solid oxide fuel cells, Int. J. Hydrogen Energy 34 (2009) 9220–9226, http://dx.doi.org/10.1016/j.ijhydene.2009.09.022.
[9] L. Da Conceição, L. Dessemond, E. Djurado, M.M.V.M. Souza, $La_{0.7}Sr_{0.3}MnO_3$-coated SS444 alloy by dip-coating process for metallic interconnect supported solid oxide fuel cells, J. Power Sources 241 (2013) 159–167, http://dx.doi.org/10.1016/j.jpowsour.2013.04.082.
[10] T. Horita, H. Kshimoto, K. Yamaji, N. Sakai, Y. Xiong, M.E. Brito, et al., Anomalous oxidation of ferritic interconnects in solid oxide fuel cells, Int. J. Hydrogen Energy 33 (2008) 3962–3969, http://dx.doi.org/10.1016/j.ijhydene.2007.07.058.
[11] F. Smeacetto, A. Chrysanthou, M. Salvo, Z. Zhang, M. Ferraris, Performance and testing of glass–ceramic sealant used to join anode-supported-electrolyte to Crofer22APU in planar solid oxide fuel cells, J. Power Sources 190 (2009) 402–407, http://dx.doi.org/10.1016/j.jpowsour.2009.01.042.
[12] C. Collins, J. Lucas, T.L. Buchanan, M. Kopczyk, A. Kayani, P.E. Gannon, et al., Chromium volatility of coated and uncoated steel interconnects for SOFCs, Surf. Coatings Technol. 201 (2006) 4467–4470, http://dx.doi.org/10.1016/j.surfcoat.2006.08.053.
[13] J. Chen, H. Yang, R. Chadeyron, D. Tang, T. Zhang, Tuning the interfacial reaction between $CaO–SrO–Al_2O_3–B_2O_3–SiO_2$ sealing glass–ceramics and Cr-containing interconnect: crystalline structure vs. glass structure, J. Eur. Ceram. Soc. 34 (2014) 1989–1996, http://dx.doi.org/10.1016/j.jeurceramsoc.2014.01.023.
[14] C. Sun, R. Hui, J. Roller, Cathode materials for solid oxide fuel cells: a review, J. Solid State Electrochem. 14 (2009) 1125–1144, http://dx.doi.org/10.1007/s10008-009-0932-0.
[15] W.Z. Zhu, S.C. Deevi, A review on the status of anode materials for solid oxide fuel cells, Mater. Sci. Eng. A 362 (2003) 228–239, http://dx.doi.org/10.1016/s0921-5093(03)00620-8.
[16] M.K. Mahapatra, K. Lu, Glass-based seals for solid oxide fuel and electrolyzer cells—a review, Mater. Sci. Eng. R Rep. 67 (2010) 65–85, http://dx.doi.org/10.1016/j.mser.2009.12.002.
[17] J.W. Fergus, Electrolytes for solid oxide fuel cells, J. Power Sources 162 (2006) 30–40, http://dx.doi.org/10.1016/j.jpowsour.2006.06.062.
[18] E.M. Levin, G.W. Cleek, Shape of liquid immiscibility volume in the system barium oxide–boric oxide–silica, J Am Ceram Soc 41 (1958) 175–179, http://dx.doi.org/10.1111/j.1151-2916.1958.tb13535.x.
[19] M. Hillert, Phase Equilibria, phase diagrams and phase transformations, Mater. Sci. (2007) 524, http://dx.doi.org/10.1017/cbo9780511812781.
[20] R.A. Chiarella, R.J. Davey, M.L. Peterson, Making co-crystals—the utility of ternary phase diagrams, Cryst. Growth Des. 7 (2007) 1223–1226, http://dx.doi.org/10.1021/cg070218y.
[21] G.N. Shabanova, V.V. Taranenkova, A.N. Korogodskaya, E.V. Khristich, Structure of the $BaO–Al_2O_3–SiO_2$ System (A review), Glass Ceram. 60 (2003) 43–46.
[22] K.T. Lee, P.B. Aswath, Kinetics of the hexacelsian to celsian transformation in barium aluminosilicates doped with CaO, Int. J. Inorg. Mater. 3 (2001) 687–692, http://dx.doi.org/10.1016/S1466-6049(01)00190-8.
[23] K.T. Lee, P.B. Aswath, Role of mineralizers on the hexacelsian to celsian transformation in the barium aluminosilicate (BAS) system, Mater. Sci. Eng. A 352 (2003) 1–7, http://dx.doi.org/10.1016/S0921-5093(02)00118-1.
[24] W.R. Foster, H.-C. Lin, System $BaO–Al_2O_3–SiO_2$. II. Binary System Celsian ($BaAl_2Si_2O_8$)-Silica (SiO2), Am. J. Sci. 267-A (1969) 134–144.
[25] C.E. Semler, W.R. Foster, System $BaO–Al_2O_3–SiO_2$. IV. The system celsian–alumina and the Join celsian–mullite, J. Am. Ceram. Soc. 52 (1969) 679–680.
[26] H.-C. Lin, W.R. Foster, System baria–alumina–silica:V. ternary system sanbornite–celsian–silica, J. Am. Ceram. Soc. 53 (1970) 549–551.
[27] E.M. Levin, H.F. McMurdie, in: M.K. Reser (Ed.), Phase Diagrams for Ceramists, 1975 Supplement, vol. III, Am. Ceram. Soc. Westerville, OH, 1975, p. 515.
[28] N. Mahato, A. Banerjee, A. Gupta, S. Omar, K. Balani, Progress in material selection for solid oxide fuel cell technology: a review, Prog. Mater. Sci. 72 (2015) 141–337, http://dx.doi.org/10.1016/j.pmatsci.2015.01.001.
[29] J. Djordjevic, V. Dondur, R. Dimitrijevic, A. Kremenovic, Structural investigations of celsian glass derived from Ba-LTA zeolite, Phys. Chem. Chem. Phys. 3 (2001) 1560–1565, http://dx.doi.org/10.1039/b009384j.
[30] Z.-H. Jiang, Q.-Y. Zhang, The structure of glass: a phase equilibrium diagram approach, Prog. Mater. Sci. 61 (2014) 144–215, http://dx.doi.org/10.1016/j.pmatsci.2013.12.001.
[31] A.R. Boccaccini, B. Hamann, In Situ high-temperature optical microscopy, J. Mater. Sci. Technol. 4 (1999) 5419–5436.
[32] C. Lara, M. Pascual, M. Prado, A. Duran, Sintering of glasses in the system $RO–Al_2O_3–BaO–SiO_2$ (R = Ca, Mg, Zn) studied by hot-stage microscopy, Solid State Ionics 170 (2004) 201–208, http://dx.doi.org/10.1016/j.ssi.2004.03.009.
[33] C.S. Ray, T. Zhang, S.T. Reis, R.K. Brow, Determining kinetic parameters for isothermal crystallization of glasses, J. Am. Ceram. Soc. 90 (2007) 769–773, http://dx.doi.org/10.1111/j. 1551-2916.2006.01478.x.
[34] S.T. Reis, M.J. Pascual, R.K. Brow, C.S. Ray, T. Zhang, Crystallization and processing of SOFC sealing glasses, J. Non Cryst. Solids 356 (2010) 3009–3012, http://dx.doi.org/10.1016/j.jnoncrysol.2010.02.028.
[35] Lee K., Aswath P.B., Enhanced production of celsian barium aluminosilicates by a three-step firing technique, 71, (2001), 47–52.
[36] De Pablos A., Duran A., Nieto M.L., Puesta a punto de un horno de fibrado de laboratorio para la obtención de fibra de vidrio. Boletín la Soc Española Cerámica Y Vidr 199, 736, 511–5.
[37] S.V. Smiljanić, S.R. Grujić, M.B. Tošić, V.D. Živanović, J.N. Stojanović, S.D. Matijašević, et al., Crystallizati on and sinterability of glass-ceramics in the system $La_2O_3–SrO–B_2O_3$, Ceram. Int. 40 (2014) 297–305, http://dx.doi.org/10.1016/j.ceramint.2013.06.002.
[38] M.O. Prado, M.L.F. Nascimento, E.D. Zanotto, On the sinterability of crystallizing glass powders, J. Non Cryst. Solids 354 (2008) 4589–4597, http://dx.doi.org/10.1016/j.jnoncrysol.2008.06.006.

[39] M.J. Da Silva, J.S. Moya, C. Pecharromán, J. Sanz, S. Mello-Castanho, High barium content lead and alkaline-free glasses, Mater. Lett. 136 (2014) 345–348, http://dx.doi.org/10.1016/j.matlet.2014.08.094.
[40] M.M. Shultz, Chemistry of glass, J. Non Cryst. Solids 73 (1985) 91–101, http://dx.doi.org/10.1016/0022-3093(85)90339-4.
[41] Y. Kim, D. Lee, W. Kim, S. Park, H. Kim, D.B. Lee, et al., Effect of glass viscosity on gas leak rate in glass seals for solid oxide fuel cell applications, Rev. Adv. Mater. Sci. 28 (2011) 111–115.
[42] J.B. Murdoch, J.F. Stebbins, I.S.E. Carmichael, High-resolution 29Si NMR study of silicate and aluminosilicate glasses: the effect of network-modifying cations, Am. Mineral. 70 (1985) 332–343.
[43] K.J. Rao, Structural chemistry of glasses, J. Am. Chem. Soc. 125 (2002) 568.
[44] A. Cozma, B. Puers, Characterization of the electrostatic bonding of silicon and Pyrex glass, J. Micromech. Microeng. 5 (1999) 98–102, http://dx.doi.org/10.1088/0960-1317/5/2/010.
[45] T. Zhang, R.K. Brow, S.T. Reis, C.S. Ray, Isothermal crystallization of a solid oxide fuel cell sealing glass by differential thermal analysis, J. Am. Ceram. Soc. 91 (2008) 3235–3239, http://dx.doi.org/10.1111/j.1551-2916.2008.02661.x.
[46] E.-S. Lim, B.-S. Kim, J.-H. Lee, J.-J. Kim, Effect of BaO content on the sintering and physical properties of $BaO–B_2O_3–SiO_2$ glasses, J. Non Cryst. Solids 352 (2006) 821–826, http://dx.doi.org/10.1016/j.jnoncrysol.2006.01.021.
[47] H.J. Schmutzler, K.H. Sandhage, Transformation of Ba–Al–Si precursors to celsian by high-temperature oxidation and annealing, Metall. Mater. Trans. B 26 (1995) 135–148, http://dx.doi.org/10.1007/BF02648986.
[48] M. Hasanuzzaman, A. Rafferty, A.G. Olabi, Effects of zircon on porous structure and alkali durability of borosilicate glasses, Ceram. Int. 40 (2014) 581–590, http://dx.doi.org/10.1016/j.ceramint.2013.06.039.
[49] J.S. Moya-Corral, A.G. Verduch, The solid solution of silica in celsian, Trans. J. Br. Ceram. Soc. 77 (1978) 40–44.
[50] Ghosh S., Kundu P., Sharma A. Das., Basu R.N., Maiti H.S. Microstructure and property evaluation of barium aluminosilicate glass–ceramic sealant for anode-supported solid oxide fuel cell, 28, (2008), 69–76. 10.1016/j.jeurceramsoc.2007.05.008.
[51] J.S. Moya-Corral, A.G. Verduch, Estudio de la reaccion entre el caolin y el carbonato de bario, Bol. La Soc. Esp. Ceram. Y Vidr. 15 (1976) 379–381.
[52] M. Kerstan, C. Rüssel, Barium silicates as high thermal expansion seals for solid oxide fuel cells studied by high-temperature X-ray diffraction (HT-XRD), J. Power Sources 196 (2011) 7578–7584, http://dx.doi.org/10.1016/j.jpowsour.2011.04.035.
[53] Bobkova N.M., Thermal Expansion of Binary Borate Glasses and Their Structure, 29, (2003), 501–7.
[54] D. Massiot, F. Fayon, V. Montouillout, N. Pellerin, J. Hiet, C. Roiland, et al., Structure and dynamics of oxide melts and glasses: a view from multinuclear and high temperature NMR, J. Non Cryst. Solids 354 (2008) 249–254, http://dx.doi.org/10.1016/j.jnoncrysol.2007.06.097.
[55] J. Schneider, V.R. Mastelaro, H. Panepucci, E.D. Zanotto, 29Si MAS-NMR studies of Qn structural units in metasilicate glasses and their nucleating ability, J. Non Cryst. Solids 273 (2000) 8–18, http://dx.doi.org/10.1016/s0022-3093(00)00139-3.
[56] T.W.T. Tsai, Y. Mou, Y.H. Tseng, L. Zhang, J.C.C. Chan, Solid-state NMR. study of bioactive binary borosilicate glasses, J. Phys. Chem. Solids 69 (2008) 2628–2633, http://dx.doi.org/10.1016/j.jpcs.2008.06.004.
[57] K. Sharma, G.P. Kothiyal, L. Montagne, F.O. Méar, B. Revel, A new formulation of barium-strontium silicate glasses and glass-ceramics for high-temperature sealant, Int. J. Hydrogen Energy 37 (2012) 11360–11369, http://dx.doi.org/10.1016/j.ijhydene.2012.04.142.
[58] L. Rezazadeh, S. Baghshahi, A.N. Golikand, Z. Hamnabard, Structure, phase formation, and wetting behavior of $BaO–SiO_2–B_2O_3$ based glass–ceramics as sealants for solid oxide fuel cells, Ionics (Kiel) 20 (2013) 55–64, http://dx.doi.org/10.1007/s11581-013-0934-x.
[59] S.E. Lin, Y.R. Cheng, W.C.J. Wei, $BaO–B_2O_3–SiO_2–Al_2O_3$ sealing glass for intermediate temperature solid oxide fuel cell, J. Non Cryst. Solids 358 (2012) 174–181, http://dx.doi.org/10.1016/j.jnoncrysol.2011.09.013.
[60] M. Kukizaki, Large-sc ale production of alkali-resistant Shirasu porous glass (SPG) membranes: influence of ZrO 2 addition on crystallization and phase separation in $Na_2O–CaO–Al_2O_3–B_2O_3–SiO_2$ glasses; and alkali durability and pore morphology of the, J. Membr. Sci. 360 (2010) 426–435, http://dx.doi.org/10.1016/j.memsci.2010.05.042.
[61] Chen A., James P.F., Section 6. physical and chemical properties of synthesized materials a morphous phase separation and crystallization in a lithium silicate glass prepared by the sol–gel method, 100, (1988) 353–8.
[62] S.K. Lee, J.F. Stebbins, Extent of intermixing among framework units in silicate glasses and melts, Geochim. Cosmochim. Acta 66 (2002) 303–309, http://dx.doi.org/10.1016/s0016-7037(01)00775-x.
[63] P. Saravanapavan, L.L. Hench, Mesoporous calcium silicate glasses. I. Synthesis, J. Non Cryst. Solids 318 (2003) 1–13, http://dx.doi.org/10.1016/s0022-3093(02)01864-1.
[64] L. Barbeeri, A.B. Corradi, C. Leonelli, T. Manfredini, M. Romagnoli, C. Siligardi, The microstructure and mechanical properties of sintered celsian and strontium–celsian glass–ceramics, Mater. Res. Bull. 30 (1995) 27–41, http://dx.doi.org/10.1016/0025-5408(94)00103-0.
[65] D. Herman, T. Okupski, W. Walkowiak, Wear resistance glass-ceramics with a gahnite phase obtained in $CaO–MgO–ZnO–Al_2O_3–B_2O_3–SiO2$ system, J. Eur. Ceram. Soc. 31 (2011) 485–492.